



Modification and evaluation of the peripheral contrast sensitivity function models

ALIAKBAR BOZORGIAN,*  MARIUS PEDERSEN, AND JEAN-BAPTISTE THOMAS

The Norwegian Color and Visual Computing Laboratory, NTNU—Norwegian University of Science and Technology, Gjøvik, Norway

*Corresponding author: ali.bozorgian@ntnu.no

Received 7 October 2021; revised 20 July 2022; accepted 27 July 2022; posted 28 July 2022; published 19 August 2022

We propose a series of modifications to the Barten contrast sensitivity function model for peripheral vision based on anatomical and psychophysical studies. These modifications result in a luminance pattern detection model that could quantitatively describe the extent of veridical pattern resolution and the aliasing zone. We evaluated our model against psychophysical measurements in peripheral vision. Our numerical assessment shows that the modified Barten leads to lower estimate errors than its original version. © 2022 Optica Publishing Group under the terms of the [Optica Open Access Publishing Agreement](#)

<https://doi.org/10.1364/JOSAA.445234>

1. INTRODUCTION

The visual area beyond the fovea is often referred to as peripheral vision. It is well known that human vision is sharp in the fovea, and acuity falls off in the periphery due to optical and neural factors [1]. One way to effectively characterize the capabilities and limitations of spatial vision in the periphery is to measure contrast detection thresholds as a function of eccentricity.

Psychophysical experiments have demonstrated that the least physical contrast required to detect a visual target varies with the target's spatial frequency [2]. This minimum physical contrast is termed the contrast detection threshold, and its reciprocal is called contrast sensitivity. If we plot contrast sensitivity as a function of the target's spatial frequency, the resulting profile would be the contrast sensitivity function (CSF) [3].

CSF could be measured for various psychophysical tasks, including detection [4] and orientation discrimination [5] of sinusoidal grating patterns. It has been shown that contrast sensitivity for detection and orientation discrimination is almost equal for gratings with spatial frequencies below the retinal Nyquist sampling limit [6]. However, beyond this limit, the orientation discrimination task (resolution) becomes impossible, while contrast detection remains possible over an aliased range of frequencies. Perception of high-frequency visual stimuli in the periphery is prone to aliasing since, unlike the fovea, the frequency content of optical images reaching the retina could exceed the Nyquist frequency of neural sampling elements [7]. In this study, we aim to derive a model of contrast threshold for detection in peripheral vision that is able to describe the limits of aliased and veridical perception over the frequency spectrum.

Various researchers have measured the peripheral CSF during the last decades [4,5,8–22]. In a typical experiment for peripheral contrast measurements, a sinusoidal grating is shown at various eccentricities to an observer whose attention is fixed

on a point. Conventionally, the presentation time of stimuli is limited to ensure that an observer does not find the time to make unintentional eye movements towards stimuli (see [4]). Chwesiuk and Mantiuk have recently suggested an alternative approach implementing an eye tracker to control gaze position [23]. This method has shown similar results and benefits from more convenience for observers.

Most studies measured contrast thresholds in normal viewing conditions; however, Hilz and Covanius employed interference fringes to bypass the eye's optics and primarily focused on the neural arrangement of the retina [17]. A common feature of the resulting curves measured either way is the decline of cutoff frequencies caused by decreased neural sampling elements in higher eccentricities [1,24].

Models of the CSF are helpful for a variety of applications. They can effectively estimate the perceptibility of images to an individual or standard observer [25]. In imaging science, various image and video compression methods exploit models of the foveal CSF to configure quantization charts [26,27]. However, in immersive gaze-contingent displays where eye tracking is possible and visual content is served to extensive degrees of the retina, implementing a foveal model of the CSF for all eccentricities is not computationally efficient [28]. Therefore, an accurate model of the peripheral CSF is beneficial for the development and enhancement of immersive gaze-contingent displays.

This study aims to modify Barten's peripheral CSF model and evaluate the results against psychophysical measurements. Section 2 provides an overview of the CSF models for peripheral vision. Section 3 discusses the neural substrate for luminance pattern perception and analyzes the assumptions made in the Barten CSF model regarding this subject. Section 4 proposes a series of modifications to the Barten CSF according to the

findings of anatomical and psychophysical studies. Section 5 elaborates on the methodologies used to evaluate the CSF models. Section 6 provides the results and discussion. Conclusions are presented in Section 7. An implementation of the CSF models in MATLAB is provided in Code 1, Ref. [29].

2. BACKGROUND

Several models of CSF are available in the literature [25,30–36]. There is often some sort of trade-off between the level of complexity and computational efficiency of the models. Simple models are more desirable; however, they do not necessarily provide the most accurate estimations of contrast thresholds [37]. Among the existing models, just a few account for peripheral contrast thresholds [28,30,33,36].

Daly implemented a multi-parameter model of contrast sensitivity in his image fidelity algorithm [33]. The model is a function of spatial frequency u in cycles per degree, orientation θ in degrees, light adaptation levels l in cd/m^2 , image size i^2 in deg^2 , lens accommodation due to distance d in meters, and eccentricity e in visual degrees:

$$S(u, \theta, l, i^2, d, e) = P(e) \times \min \left[S \left(\frac{u}{bw_a, bw_e, bw_\theta}, l, i^2 \right), S(u, l, i^2) \right], \quad (1)$$

where S is sensitivity, and $P(e)$ corresponds to the absolute peak of the sensitivity curve and is a function of eccentricity [38]. The parameters bw_a , bw_e , and bw_θ scale bandwidth as a function of lens accommodation, eccentricity, and orientation, respectively:

$$P(e) = 250 \times \left(\frac{1}{1 + ke} \right), \quad (2)$$

$$bw_a = 0.856 \times d^{0.14}, \quad (3)$$

$$bw_e = \frac{1}{1 + ke}, \quad (4)$$

$$bw_\theta = \left(\frac{1 - ob}{2} \right) \times \cos(4\theta) + \frac{1 + ob}{2}, \quad (5)$$

where $k = 0.24$ and $ob = 0.7$.

The sensitivity is defined as a function of frequency, light adaptation, and image size:

$$S(u, l, i^2) = ((3.23 \times (u^2 i^2)^{-0.3})^5 + 1)^{-0.2} \times A_1 \varepsilon u \exp(-B_1 \varepsilon u) \sqrt{1 + 0.06 \times \exp(B_1 \varepsilon u)}, \quad (6)$$

$$A_1 = 0.801 \times \left(1 + \frac{0.7}{l} \right)^{-0.2}, \quad (7)$$

$$B_1 = 0.3 \times \left(1 + \frac{100}{l} \right)^{0.15}, \quad (8)$$

where ε equals 0.9 for achromatic CSF. The first half of Eq. (6) deals with sensitivity changes as a function of image size, while

the second half deals with sensitivity and bandwidth changes as a function of light adaptation and is based on an earlier empirical model proposed by Barten [39].

Barten [30] and Rovamo *et al.* [31] have proposed analytical CSF models based on the principles of signal detection theory. Both models assume that contrast sensitivity is determined mainly by the modulation transfer function (MTF) of the eye, lateral inhibition, and internal noise of the visual system. Rovamo *et al.* focused on the effect of the grating area and spatial integration, while Barten provided a more comprehensive treatment of other factors, including eccentricity.

The following expression forms the basis for the Barten CSF model:

$$S(u) = \frac{1}{m_t(u)} = \frac{M_{\text{opt}}(u)}{2k} \times \sqrt{\frac{XYT}{\Phi_{\text{ph}} + \frac{\Phi_0}{M_{\text{lat}}^2(u)}}}, \quad (9)$$

where u is spatial frequency expressed in cycles per degree, $S(u)$ is the CSF, $m_t(u)$ is the modulation threshold, $M_{\text{opt}}(u)$ is the optical MTF of the eye, k is a constant similar to signal-to-noise ratio, X , Y , and T are spatial and temporal dimensions of the object, Φ_{ph} is the photon noise, Φ_0 is the neural noise, and M_{lat} is the MTF of the lateral inhibition process.

To extend Barten's CSF model to peripheral vision, it might be sufficient to adapt each parameter of Eq. (9) based on eccentricity. The actual factor mediating CSF variation with eccentricity is spatial integration over the receptive field area of ganglion cells [4,8,19]. It is well known that the density of receptive fields declines in the retinal periphery, while the receptive field area increases with eccentricity [1]. However, the density of receptive fields and receptive field area are two independent features of a cell mosaic, and their product is called the coverage factor [40]. Barten presumed that the variation of the parameters with eccentricity is caused mainly by density variation of on-center M ganglion cells over the retina. Relying on density, rather than receptive field area, as the primary variable of interest could be justified by making an additional assumption that the coverage factor of the target subgroup of ganglion cells is constant and equal to one across the retina. A coverage factor of one corresponds to no gap or overlap among the mosaic of the cells. A coverage factor above one implies overlap among neighboring cells, while a coverage factor below one describes a mosaic cell that contains gaps [41]. Barten proposed the following approximation formula for average density variation of on-center M ganglion cells in all four hemifields:

$$N_{M-\text{on}} = F_{M-\text{on}} \times N_{g0} \times \left(\frac{0.85}{1 + \left(\frac{e}{0.45}\right)^2} + \frac{0.15}{1 + \left(\frac{e}{e_g}\right)^2} \right), \quad (10)$$

where $N_{M-\text{on}}$ is the density of on-center M cells, $F_{M-\text{on}}$ is the fraction of retinal ganglion cells that are M type and have on-center receptive fields (assumed to be the constant value of 0.05 according to primate data [42]), N_{g0} is the density of total retinal ganglion cells in the fovea, e is the eccentricity in visual degrees, and e_g is a constant equal to 3.3 deg. It is well established that the density of retinal ganglion cell bodies is zero in the fovea due to the Henle effect [43]. Therefore, the value N_{g0} represents the number of foveal receptive fields associated with displaced central ganglion cell bodies.

According to Barten, the optical MTF aims to describe not only the filtering characteristics of the lens, but also the effects of stray light in the ocular media, diffraction in the retina, and discrete structure of the photoreceptors. Based on the central limit theorem, the combined effect of several lowpass MTFs could be characterized by a Gaussian function [44]. Therefore, Barten assumed that the optical MTF of the eye can be approximated by

$$M_{\text{opt}}(u) = \exp(-2\pi\sigma^2 u^2), \quad (11)$$

where σ is the standard deviation of the point spread function (PSF) resulting from the convolution of several other PSFs, each describing the various stages of filtering mentioned above (assuming linearity). If PSFs are entirely positive and normalized to unit volume, then the variance of their convolution is equal to the sum of the variances of each individual spread function [45]. Therefore, σ could be computed from the following expressions:

$$\sigma_0 = \sqrt{\sigma_{00}^2 + \sigma_{\text{ret}}^2} \quad (12)$$

and

$$\sigma = \sqrt{\sigma_0^2 + (C_{ab}d)^2}, \quad (13)$$

where σ_{ret} is the standard deviation of the spread function caused by the discrete structure of the retina, σ_{00} is the standard deviation of a PSF describing the remaining parts of σ_0 , C_{ab} is a constant describing the increase of σ at increasing pupil size, and d is the pupil diameter in mm. The quantity σ_{ret} is a function of $N_{M-\text{on}}$ based on the following expression:

$$\sigma_{\text{ret}} = \frac{1}{\sqrt{7.2\sqrt{3} N_{M-\text{on}}}}. \quad (14)$$

Neural noise, which is assumed to be generated from the statistical variation of the signals in nerve fibers conveying visual information to the visual cortex, is calculated from

$$\Phi_0(e) = \Phi_{00} \times \frac{N_{M-\text{on}}(0)}{N_{M-\text{on}}}, \quad (15)$$

where Φ_{00} is the value of neural noise at foveal vision.

The MTF of the lateral inhibition process, which attenuates sensitivity at low frequencies, is empirically described by the following approximation formula:

$$M_{\text{lat}}(u) = \sqrt{1 - e^{-\left(\frac{u}{u_0(e)}\right)^2}}, \quad (16)$$

where u_0 is the spatial frequency that lateral inhibition ceases as a function of eccentricity. From an analysis of peripheral CSF measurement, it might be assumed that u_0 is described by the following equation:

$$u_0(e) = u_0(0) \cdot \left(\frac{N_{M-\text{on}}(0)}{N_{M-\text{on}}}\right)^{0.5} \times \left(\frac{0.85}{1 + \left(\frac{e}{4}\right)^2} + \frac{0.13}{1 + \left(\frac{e}{20}\right)^2} + 0.02\right)^{-0.5}, \quad (17)$$

where $u_0(0)$ is the spatial frequency at which lateral inhibition ceases in the fovea. The second term characterizes the effect of an increased receptive field diameter at higher eccentricities, and the third term induces the effect of decreasing the number of ganglion cells engaging in the lateral inhibition process.

According to the definition implemented in Barten's model, quantum efficiency of the eye is defined as the mean number of photons causing activation of cones divided by the total number of photons entering the pupil. The following approximation formula might be used to describe the variation of quantum efficiency by eccentricity:

$$\eta(e) = \eta_0 \left(\frac{0.4}{1 + \left(\frac{e}{7}\right)^2} + \frac{0.48}{1 + \left(\frac{e}{20}\right)^2} + 0.12 \right), \quad (18)$$

where η_0 denotes quantum efficiency in the fovea.

The human eye seems to have limited ability to integrate signals over temporal and spatial dimensions and compare them with noise. For integration time of the eye, Schade proposed a value of 0.1 s for almost all luminance levels [2]. It is assumed here that the presentation time of the stimuli is longer than the integration time of the eye; therefore, T equals 0.1 s. Barten did not adapt T based on eccentricity. However, the following equations hold for spatial dimensions:

$$X = \left(\frac{1}{X_0^2} + \frac{1}{X_{\text{max}}^2} + \frac{(0.5X_0)^2 + 4e^2}{(0.5X_0)^2 + e^2} \frac{u^2}{N_{\text{max}}^2} \right)^{-0.5} \quad (19)$$

and

$$Y = \left(\frac{1}{Y_0^2} + \frac{1}{Y_{\text{max}}^2} + \frac{(0.5X_0)^2}{(0.5X_0)^2 + e^2} \frac{u^2}{N_{\text{max}}^2} \right)^{-0.5}, \quad (20)$$

where X_0 and Y_0 are dimensions of the object, X_{max} and Y_{max} are maximum integration areas of the eye, and N_{max} is the maximum number of cycles that the human eye can perform integration over. It is assumed that X_{max} and Y_{max} are a function of eccentricity based on the following approximation formula:

$$X_{\text{max}}(e) = Y_{\text{max}}(e) = X_{\text{max}}(0) \left(\frac{0.85}{1 + \left(\frac{e}{4}\right)^2} + \frac{0.15}{1 + \left(\frac{e}{12}\right)^2} \right)^{-0.5}, \quad (21)$$

where $X_{\text{max}}(0)$ denotes the maximum integration area in the fovea. The typical values for the parameters in Barten's peripheral CSF model are given in Table 1.

The performance of a CSF model is often evaluated based on how accurately it can estimate experimental contrast thresholds [28,30,32,46]. Barten provided a qualitative graphical evaluation of his CSF model against experimental datasets available at the time [30]. However, there is a problem with the way the model was evaluated. Whenever resulting curves from

Table 1. Typical Values for Parameters and Constants Used in Barten CSF Model [30]

Parameter	Value	Parameter	Value	Parameter	Value
k	3.0	T [sec]	0.1	η_{00}	0.03
σ_0 [arc min]	0.5	$X_{\text{max}}(0)$ [deg]	12	Φ_{00} [sec deg ²]	3×10^{-8}
C_{ab} _[$\frac{\text{arc min}}{\text{mm}}$]	0.08	N_{max} [cycles]	15	$u_0(0)$ _[$\frac{\text{cycles}}{\text{deg}}$]	7

the model were compared with a specific experimental dataset, ganglion cell density values were manually manipulated to give the best fit to high-frequency data points at each eccentricity.

3. NEURAL SUBSTRATE FOR ACHROMATIC CONTRAST SENSITIVITY FUNCTION

Barten's model is based on various assumptions regarding the optical performance of the eye and the anatomical structure of the retinal cells. Most of these assumptions lead to a reasonable estimation of the contrast thresholds; nonetheless, some aspects might need reconsideration to achieve more accurate results. This section will first discuss the role of ganglion cells on peripheral contrast sensitivity in Barten's model and then present a body of evidence that suggests potential modifications to the model.

It is well established that the number of retinal ganglion cells decreases as a function of eccentricity in para-foveal regions [1]. Barten postulated that the density variation of ganglion cells plays the most crucial role in the variation of contrast sensitivity with eccentricity [30]. Correspondingly, to extend his model of CSF to higher eccentricities, he adapted each parameter of the foveal model based on the density variation of ganglion cells [see Eqs. (9)–(21)]. As mentioned earlier, ganglion cell density influences the actual factor of importance, spatial summation [4,8,19], only indirectly because of the link between density and receptive field area (assuming a constant coverage factor). Furthermore, it is assumed that only on-center M ganglion cells, corresponding to 0.05% of the total population, are responsible for the luminance channel. However, there is a lack of consensus on the relevant type of ganglion cells for the luminance channel in the literature (for a review, see [47]).

Various retinal ganglion cells relay visual signals in parallel neural pathways from the retina to the lateral geniculate nucleus (LGN). Each cell type is distributed throughout the retina and forms an independent network of sampling elements. Therefore, the overall activity of each network forms a distinct representation of the visual world [48]. For the primate retina, 80% of the ganglion cells are identified as midget cells terminating in parvocellular layers of LGN, forming the P pathway; 10% are Parasol cells (M cells) terminating in magnocellular layers, forming the M pathway, and others belong to the K pathway [42]. The parvocellular and magnocellular pathways maintain their crisp anatomical separation until the striate cortex and remain somewhat segregated in higher levels as well [49].

A widespread hypothesis in vision science associates subcortical pathways with distinct visual functions [50]. These suggestions are based on lesion studies or the clustering of physiological and anatomical features in the three main visual pathways [51]. However, the cumulative evidence from physiological and anatomical studies has failed to associate a single subcortical pathway with the luminance pattern perception and subsequently achromatic contrast sensitivity.

Physiological studies often promote the view that M cells are a favorable origin of the luminance channel [47,52,53], especially at low-contrast levels near the perceptual detection thresholds [54]. However, these reports lack any consideration of retinal sampling and the fact that contrast of the under-sampled patterns remains detectable beyond the Nyquist limit, as proven by the perceptual visibility of aliasing in the peripheral retina

[55]. For the human CSFs measured in this older literature, no data were obtained for gratings beyond the retinal Nyquist limits established by Wilkinson *et al.* [56]. Similarly, contrast sensitivities less than 10 that are most relevant to aliased percepts were not reported.

Anatomical studies have suggested that the M cell mosaic is not dense enough to support the resolving ability of macaque or human observers for high-frequency luminance patterns [47]. On the other hand, the Nyquist frequency of the P mosaic in human and macaque retinas closely follows veridical measures of acuity, rendering the P pathway as a favorable origin for fine luminance pattern resolution [56–60]. Moreover, spatial summation over M cells' relatively large receptive fields substantially attenuates their responses for spatial frequencies above the Nyquist limit. Only P cells have receptive fields small enough to continue signaling the presence of spatial contrast at high spatial frequencies beyond the Nyquist limit of their own array.

To reconcile the findings related to the neural origin of the achromatic CSF, the best strategy might be to take a step back and resist the desire to associate a single pathway for luminance pattern vision. In this view, both M and P pathways may contribute to the detection of luminance gratings. The high-gain M cells are well suited for detecting luminance patterns at low to medium spatial frequencies, while the condensed mosaic of P cells provides required sampling elements for resolution of high-frequency patterns up to the Nyquist limit and maintaining detection of percepts in the aliasing zone [54,61]. Such notion is in concert with lesion studies of primates (for a review, see [49]), where localized lesions of magnocellular layers in LGN resulted in a loss of sensitivity in lower spatial frequencies, and localized lesions of parvocellular layers in LGN caused loss of sensitivity in higher spatial frequencies.

4. MODIFIED BARTEN CSF FOR PATTERN DETECTION AND RESOLUTION

Although Barten did not address this controversy and solely associated M cells with the achromatic CSF (he was possibly motivated by the parallel neural pathways hypothesis), the modular nature of his model provides the means for reflecting the composite contribution of M and P cells. To obtain a hybrid CSF model for pattern detection, it might be sufficient to modify the optical MTF of the eye, which mediates the high-frequency region of the CSF curve.

Thibos *et al.* measured the maximum spatial frequency for the resolution and detection of luminance patterns using interference fringes. From the quantitative comparison of their data with morphology and physiology of retinal cells, it was concluded that pattern resolution is limited by the spacing of primate P cells, while the size of individual cones limits pattern detection [55,57].

A. Pattern Detection

To model limits of pattern detection, including aliasing percepts, we may rely on the radius of cones as the main parameter of interest to determine the σ_{ret} value in Eq. (12). If we assume a hexagonal array of cone sampling throughout the retina, the distance between two neighboring rows of cones is given by

$$s = \frac{1}{2}\sqrt{3}d, \quad (22)$$

where d is the center-to-center distance of the cones. We acknowledge that a hexagonal arrangement for cone sampling is valid only for the central retina, where rods are less present, and cones are tightly packed. However, we assume a virtual hexagonal array of cones in higher eccentricities with the condition $d = 2r_c$, where r_c is the cone radius. The spacing in this virtual hexagonal array is determined by the radius of individual cones rather than their population density. This assumption enables us to account for the findings of Thibos *et al.* [57] without adding further complexity to the model. According to Barten, the parameter σ_{ret} is determined by the size of the elementary area that performs spatial summation and delivers information to the brain. In the virtual hexagonal array, rows of cones form the line-spread function (LSF) that determines the effect of the neural structure on the optical MTF of the eye. The half-width of the LSF is equal to the row spacing of the cones (see Fig. 4.7 in [30]). From the geometrical configuration of the virtual hexagonal array, it can be derived that

$$\sigma_{\text{ret}} = \frac{r_c}{\sqrt{18/5}}. \quad (23)$$

Thibos *et al.* estimated variation of the cone radius as a function of eccentricity based on measurements of Polyak [62] by the following function (line equation extracted from Fig. 3 in [57] using WebPlotDigitizer software [63]):

$$r_c = 0.45/30e + 0.25, \quad (24)$$

where e is eccentricity in visual degrees. Similarly, Jonas *et al.* [64] reported a value of 0.33 arcmin for the cone radius at the fovea and 1 arcmin in the outer retinal regions. We do not account for possible asymmetries between the radii of cones in different meridians. Finally, by substituting Eq. (14) with Eq. (23) a modified CSF curve is obtained capable of predicting limits of pattern detection.

B. Limits of Pattern Resolution and the Extent of Aliasing Zone

To model the limits of veridical pattern resolution, we may rely on the density variation of P cells as the main parameter of interest [56]. Watson proposed a formula for the density distribution of human midget (P) receptive fields as a function of eccentricity [60]. We favor this formula over that of Barten [Eq. (10)] since it accounts for the density asymmetry of ganglion cells in the principal meridians, offers an improved treatment of the Henle effect building upon the study of Drasdo *et al.* [43], and can be extended for arbitrary retinal locations. The following expression describes the density of midget (P) receptive fields:

$$d_{mf}(r, k) = 2d_c(0) \left(1 + \frac{r}{r_m}\right)^{-1} \times \left[a_k \left(1 + \frac{r}{r_{2,k}}\right)^{-2} + (1 - a_k) e^{-\frac{r}{r_{e,k}}} \right], \quad (25)$$

where r is eccentricity expressed in visual degrees, k is an index indicating the principal meridian, $d_c(0)$ is the foveal density of

Table 2. Parameter Values for Eq. (25), Adapted from Watson [60]

Meridians	Parameters			
	k	a	r_2	r_e
Temporal	1	0.9851	1.058	22.14
Superior	2	0.9935	1.035	16.35
Nasal	3	0.9729	1.084	7.633
Inferior	4	0.9660	0.9932	12.13

cones, r_m is the eccentricity at which midget (P) cells comprise half of the total population of ganglion cells, $r_{2,k}$ is the eccentricity in meridian k at which density is decreased by a factor of four, a_k is a weighting factor, and $r_{e,k}$ is the scale factor of the exponential in meridian k . Table 2 reports numerical values for parameters in each of the four meridians.

The midget (P) ganglion cells can be divided into two distinct cell types, based on how deep their dendrites stratify in the inner plexiform layer (IPL). One type stratifies in the inner portion of IPL, and the other type stratifies in the outer portion of IPL, corresponding to ON and OFF cells identified physiologically. It is expected that each of these cell types establishes two independent mosaics of cell bodies across the retina with a coverage factor of one [59,65]. Watson's formula provides an estimation for the combined population of ON and OFF P cells. In the derivation process of the formula, it was assumed that ON and OFF cells each comprise half of the total population, neglecting reports of asymmetry.

Wilkinson *et al.* measured the bandwidth of veridical resolution by using monochromatic interference fringes to stimulate various locations of the retina with high-contrast sinusoidal gratings. From a quantitative comparison of their results to the density of ganglion cells, it was concluded that Nyquist limits imposed by 50% of P cells in Watson's formula are in close agreement with pattern resolution limits obtained beyond the parafoveal region [56]. Assuming a hexagonal arrangement for the P cells over the retina, the upper limit of veridical pattern resolution and the onset of the aliasing zone is derived by the following expression [60]:

$$N = \sqrt{\frac{0.5d_{mf}(r, k)}{2\sqrt{3}}}, \quad (26)$$

where N is the Nyquist frequency obtained from 50% of P cells. It has been reported that sensitivity for contrast resolution falls abruptly near the veridical limit [7]. Therefore, we will demonstrate sensitivity fall-off at the Nyquist limits with vertical lines in our modified model.

C. Neural Noise in Peripheral Vision

Neural noise is assumed to rise from the statistical fluctuation of the signals in the nerve fibers transporting luminance information to the brain. Barten relied on the following expression to model variation of neural noise in periphery [30]:

$$\Phi_0 = \sigma^2 \Delta x \Delta y \Delta t = \frac{\sigma^2 \Delta t}{N_{M-\text{on}}}, \quad (27)$$

where $\Delta x \Delta y$ is the retinal angular area covered by one nerve fiber, and Δt is the integration time of the human visual system. $\Delta x \Delta y$ has been replaced by $1/N_g$, where N_{M-on} is the density of the on-center M cells. In this formula, σ is the relative standard deviation of the signal carried by an individual nerve fiber to the brain. If σ and Δt are assumed to not vary with eccentricity, this expression implies that the spectral density of neural noise changes inversely proportionally to the density of ganglion cells. This means that the spectral density of the neural noise can be modeled as a function of eccentricity by Eq. (15). However, we have two main concerns regarding the validity of the assumptions made in the derivation process explained above. First, as discussed in the previous section, both M and P cells are likely to be responsible for luminance perception; therefore, one may not solely rely on the density variation of the on-center M cells in estimating the neural noise parameter. Second, replacing $\Delta x \Delta y$ with $1/N_g$ is valid only when the coverage factor is constant through the retina and equal to one. Although there has been evidence for a coverage factor of constant one for P cells [59], such conditions do not hold for M cells. Yamada *et al.* reported a variation in the coverage factor of M cells from central to mid periphery [66]. These concerns cast doubt on the validity of estimations made by Eq. (15) for neural noise.

Daly showed that a cortical magnification model could sufficiently estimate normalized peak sensitivity across the visual field [38]. Since variation of peak sensitivity is mediated mainly by the neural noise parameter in the Barten CSF, it may also be concluded that a cortical magnification model can sufficiently estimate the variation of the neural noise across the visual field. Subsequently, we propose the following expression for neural noise ($k = 0.24$):

$$\Phi_0 = \Phi_{00} \times (1 + ke). \quad (28)$$

Note that our modification is motivated mainly by comparing the resulting curves from the Barten CSF to the empirical measurements of contrast sensitivity in peripheral regions [8,18].

5. METHODS

A. Experimental Data for Evaluation

Thibos *et al.* performed several experiments to characterize aliasing in peripheral vision [7]. They measured psychometric functions for resolution and detection tasks in several eccentricities. Moreover, CSFs for detection and resolution were measured at 30 deg of eccentricity on the horizontal meridian of the nasal visual field. The stimulus was a stationary sinusoidal grating with a mean luminance of 80 cd/m² generated on a calibrated monitor. Subjects observed the stimulus through a circular aperture of the same mean luminance. The diameter of the gratings varied from 0.67 deg (foveal), 1.33 deg (10 deg of eccentricity), to 2.67 deg (20 or 30 deg eccentricity). Three subjects participated in the experiments. Peripheral refractive errors were carefully corrected. Data points were collected from figures of the original paper using WebPlotDigitizer software [63].

B. Parameters and Constants in Daly's CSF Model

According to Daly [33], the absolute peak of contrast sensitivity curves [parameter P in Eq. (1)] varies from observer to observer. From an investigation of experimentally measured CSF for a large population of observers [67], a value of 250 was suggested for the general implementation of the model. We did not fit the parameter values in the model to the evaluation data points and relied on the typical values reported in the original paper.

C. Parameters and Constants in Barten's CSF Model

According to Barten [30], when the CSF model is compared to experimental measurement, σ_0 , η_{00} , and k might need to be optimized based on trial and error to attain the best fit with measurements. σ_0 seems to influence the high-spatial-frequency section of the curve, η_{00} seems to influence middle spatial frequencies, and k seems to influence low spatial frequencies. However, we do not fit these parameters to the evaluation data points and rely on the typical values reported in Table 1.

D. Performance Measure

The standard error of the estimate is used to measure the typical size of model prediction errors across all frequencies in the units of contrast sensitivity. The standard error of the estimate for a sample of data is calculated by the following expression [68]:

$$\sigma_{\text{est}} = \sqrt{\frac{\sum (Y - \hat{Y})^2}{N - 2}}, \quad (29)$$

where Y is actual (experimental) data points, \hat{Y} is fitted (model) values, and N is the number of samples.

6. RESULTS

A. Graphical Comparison of the CSF Models

Figure 1 compares Daly's, original Barten, and modified Barten CSFs for eccentricities ranging from zero to 30 visual degrees. All models are set to binocular mode, and the resolution limit is derived from taking the average of nasal and temporal Nyquist limits estimated by Watson's 50% model.

1. Original Barten CSF against Modified Barten CSF

In the fovea, original and modified versions of Barten's CSFs overlay entirely. However, two significant distinctions appear between the resulting curves in higher eccentricities. First, the modified version maintains higher sensitivity values than the original version. Second, the modified version sustains a higher bandwidth than the original version. The first effect is believed to arise from the modification introduced to the neural noise term through Eq. (28), and the second effect is rooted in the modification applied to the optical MTF through Eqs. (23) and (24). Note that gray vertical lines predict limits to the pattern resolution. These lines are obtained by taking into account 50% of P cells in Watson's mathematical formula. In the fovea, the gray line exceeds the cutoff frequency of both curves. This prediction agrees with previous studies reporting that pattern detection and resolution in the fovea are limited by the filtering

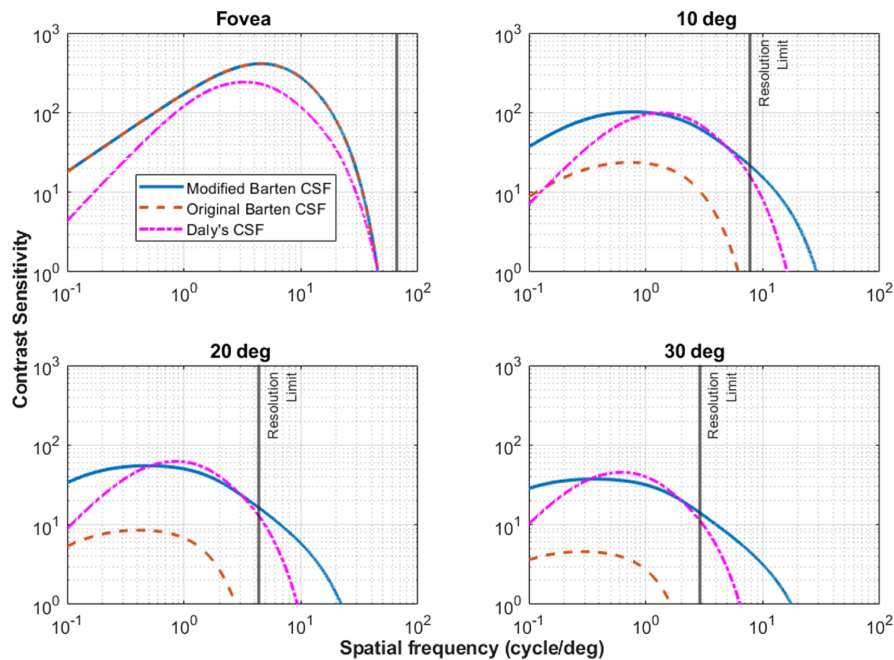


Fig. 1. Comparison among Daly's, original Barten, and modified Barten CSF models for zero to 30 eccentricities in binocular mode. The blue, red dashed, and magenta dashed-dotted lines denote sensitivity values derived from modified Barten, original Barten and Daly's CSF, respectively. The vertical gray lines show the resolution limits imposed by the Nyquist frequency of P cells when half of their population is considered. While two models overlap entirely in the fovea, the modified version sustains a higher sensitivity and bandwidth in higher eccentricities. The area between the cut-off frequency of the modified Barten and the resolution limit denotes the aliasing zone. The parameters in both original and modified versions were adjusted based on the typical values reported in Table 1. The luminance and field diameter constants are set to 150 candela per square meter and five visual degrees, respectively.

effect of optical aberrations and diffraction rather than retinal sampling [69,70]. In higher eccentricities, however, the gray lines are shifted below the cutoff frequency values obtained from modified Barten. The visual stimuli with frequencies higher than the resolution limit are predicted to remain detectable but would be perceived with aliasing artifacts. The area between the resolution limit and cutoff frequency of modified Barten is an estimation of the aliasing zone. The cutoff frequencies derived from the original Barten are consistently below the gray lines.

2. Daly's CSF against Original and Modified Barten

In the fovea, Daly's CSF has a lower peak sensitivity than other models; however, their cutoff frequencies are very close. In the peripheral vision, the peak sensitivity values resulting from Daly's and the modified version of the Barten CSF match closely. This is not the case with the original Barten. The cutoff frequency of Daly's CSF in higher eccentricities consistently exceeds the predicted retinal Nyquist limits by Watson's mathematical formula.

3. Evaluation against Psychophysical Measurements

Figure 2 compares Daly's, original Barten, and modified Barten CSFs against psychophysical measurements of the pattern resolution and detection by Thibos *et al.* in 30 visual degrees of eccentricity [7]. The luminance and diameter for all models are set to 80 cd/m^2 and 2.67 deg, respectively. Original and modified versions of the Barten CSF are set to monocular

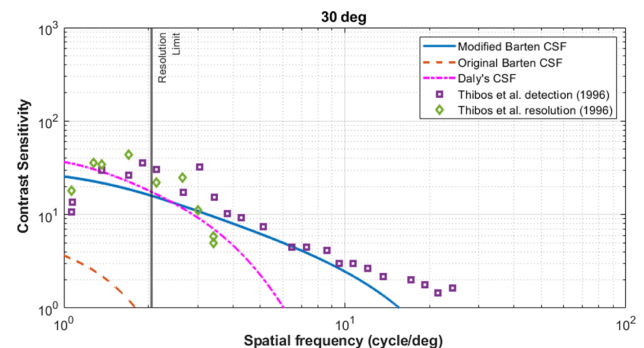


Fig. 2. Comparison of the Daly's, original Barten, and modified Barten CSF against psychophysical measurements of pattern detection and resolution by Thibos *et al.* [7]. The blue, red dashed, and magenta dashed-dotted lines denote modified Barten, original Barten, and Daly CSF, respectively. The purple squares and green diamonds correspond to the pattern detection and resolution measurements, respectively. The modified Barten CSF can follow extended data points through the aliasing zone.

mode. These parameter values are chosen to simulate the viewing conditions under which the psychophysical experiment was done.

Two main features in the measurements of Thibos *et al.* are of primary importance to us: first, the limit of pattern resolution beyond which observers start to report aliased percepts; second, the extended tail of pattern detection below 10 units of contrast sensitivity through the aliasing zone. As evident from the figure, the modified Barten CSF can somewhat describe

Table 3. Standard Error of Estimate of CSF Models for Detection and Resolution in 30 deg of Eccentricity

CSF Model	Standard Error of the Estimate for Detection	Standard Error of the Estimate for Resolution
	Data Points	Data Points
Original Barten	16.45	28.15
Modified Barten	8.59	—
Daly	10.55	11.93

both features. The mismatch between the cutoff frequency of the modified Barten and the detection task might be due to the asymmetries in the radii of cones between principal retinal meridians. Another possibility is that the typical value reported for the maximum number of cycles in Table 1 is underestimated. Barten observed an extensive range of values for this parameter after fitting the model to several foveal datasets ($N_{\max} = 5$ to $N_{\max} = 25$) [30]. However, he proposed $N_{\max} = 15$ for a typical usage of the model. Higher values could improve the performance of the modified Barten CSF; however, we relied on the typical value for the sake of a fair comparison between different models.

The original implementation of the Barten CSF underestimates sensitivity values by a large margin and fails to estimate both resolution and detection data points. This effect is due mainly to the neural noise term implemented in the model that leads to very low contrast sensitivities in the periphery.

Daly's CSF follows the resolution data points in the high-sensitivity region; however, it fails to follow either detection or resolution data points in the low-sensitivity region. We expected such behavior from Daly's CSF since peak sensitivity values and bandwidth are both scaled based on a spatial scale model [71]. Obtaining peripheral CSF for detection based on scaling is shown to be inaccurate since the shapes of foveal and peripheral CSF curves do not match [7]. None of the CSF models can predict the sensitivity attenuation seen in the range of 1 to 2 cpds. The sensitivity attenuation due to the lateral inhibition in the CSF models is usually observed below 1 cpd.

The standard errors of the estimate resulting from the CSF models in 30 deg of eccentricity are reported in Table 3. This measure describes how accurate each model was in estimating the psychophysical measurements. Note that we do not report the standard error of the estimate for the modified Barten in the resolution task. This is because the modified Barten is not supposed to predict the sensitivity fall-off at the retinal Nyquist limit in the resolution task by definition.

In agreement with the graphical comparison, the standard error of the estimate demonstrates that the modified Barten CSF results in the lowest estimate error for the detection task. The resolution limit predicted by the Nyquist frequency of 50% of P cells in the nasal visual field of the right eye (2.05 cpd) is lower than the resolution limit reported by Thibos *et al.* (3.2 cpd) or Wilkinson *et al.* (3.67 cpd) at the same retinal location. Additional psychophysical measurements in other eccentricities are required for further investigation of the model's performance.

7. CONCLUSION

A series of modifications was introduced to the Barten CSF model for peripheral vision. These modifications include the change of optical MTF, and neural noise term. The limit of pattern resolution and the aliasing zone were also modeled based on a mathematical density distribution formula for P ganglion cells. Our numerical and graphical comparison to the psychophysical measurement of sensitivity curves in the periphery shows that out of the CSF models investigated, the modified Barten results in the lowest error of the estimate for the detection task. The main advantage of our model is its ability to model the limit of pattern resolution and the extended tail of pattern detection through the aliasing zone.

Disclosures. The authors declare no conflicts of interest.

Data availability. Data underlying the results presented in this paper are available in [7,56,57]. Resulting data from CSF models are accessible through the MATLAB codes provided in Code 1, Ref. [29].

REFERENCES

- C. A. Curcio and K. A. Allen, "Topography of ganglion cells in human retina," *J. Comp. Neurol.* **300**, 5–25 (1990).
- O. H. Schade, "Optical and photoelectric analog of the eye," *J. Opt. Soc. Am.* **46**, 721–739 (1956).
- D. M. Chandler, "Seven challenges in image quality assessment: past, present, and future research," *ISRN Signal Process.* **2013**, 1–53 (2013).
- J. S. Pointer and R. F. Hess, "The contrast sensitivity gradient across the human visual field: with emphasis on the low spatial frequency range," *Vision Res.* **29**, 1133–1151 (1989).
- E. Peli, J. Yang, and R. B. Goldstein, "Image invariance with changes in size: the role of peripheral contrast thresholds," *J. Opt. Soc. Am. A* **8**, 1762–1774 (1991).
- A. B. Watson and J. G. Robson, "Discrimination at threshold: labelled detectors in human vision," *Vision Res.* **21**, 1115–1122 (1981).
- L. N. Thibos, D. L. Still, and A. Bradley, "Characterization of spatial aliasing and contrast sensitivity in peripheral vision," *Vision Res.* **36**, 249–258 (1996).
- A. Johnston, "Spatial scaling of central and peripheral contrast-sensitivity functions," *J. Opt. Soc. Am. A* **4**, 1583–1593 (1987).
- S. J. Anderson, K. T. Mullen, and R. F. Hess, "Human peripheral spatial resolution for achromatic and chromatic stimuli: limits imposed by optical and retinal factors," *J. Physiol.* **442**, 47–64 (1991).
- M. S. Banks, A. B. Sekuler, and S. J. Anderson, "Peripheral spatial vision: limits imposed by optics, photoreceptors, and receptor pooling," *J. Opt. Soc. Am. A* **8**, 1775–1787 (1991).
- K. T. Mullen, "Colour vision as a post-receptoral specialization of the central visual field," *Vision Res.* **31**, 119–130 (1991).
- K. T. Mullen and F. A. A. Kingdom, "Differential distributions of red-green and blue-yellow cone opponency across the visual field," *Vis. Neurosci.* **19**, 109–118 (2002).
- K. T. Mullen, M. Sakurai, and W. Chu, "Does L/M cone opponency disappear in human periphery?" in *Perception* (SAGE, 2005), Vol. **34**, pp. 951–959.
- M. Chwesiuk and R. Mantiuk, "Measurements of contrast sensitivity for peripheral vision," in *ACM Conference on Applied Perception* (2019).
- J. M. Ditch and D. G. Green, "Contrast sensitivity of the human peripheral retina," *Vision Res.* **9**, 947–952 (1969).
- L. Ronchi and G. Fidanzi, "Changes of psychophysical organization across the light-adapted retina," *J. Opt. Soc. Am.* **62**, 912–915 (1972).
- R. Hiltz and C. R. Cavonius, "Functional organization of the peripheral retina: sensitivity to periodic stimuli," *Vision Res.* **14**, 1333–1337 (1974).

18. V. Virsu and J. Rovamo, "Visual resolution, contrast sensitivity, and the cortical magnification factor," *Exp. Brain Res.* **37**, 475–494 (1979).
19. J. G. Robson and N. Graham, "Probability summation and regional variation in contrast sensitivity across the visual field," *Vision Res.* **21**, 409–418 (1981).
20. D. H. Kelly, "Retinal inhomogeneity. I. Spatiotemporal contrast sensitivity," *J. Opt. Soc. Am. A* **1**, 107–113 (1984).
21. M. W. Cannon, "Perceived contrast in the fovea and periphery," *J. Opt. Soc. Am. A* **2**, 1760–1768 (1985).
22. M. J. Mayer and C. W. Tyler, "Invariance of the slope of the psychometric function with spatial summation," *J. Opt. Soc. Am. A* **3**, 1166–1172 (1986).
23. M. Chwesiuk and R. Mantiuk, "Measurements of contrast detection thresholds for peripheral vision using non-flashing stimuli," in *Smart Innovation, Systems and Technologies* (2018), Vol. **73**, pp. 258–267.
24. Y. Z. Wang, L. N. Thibos, and A. Bradley, "Effects of refractive error on detection acuity and resolution acuity in peripheral vision," *Investig. Ophthalmol. Vis. Sci.* **38**, 2134–2143 (1997).
25. P. G. J. Barten, "Formula for the contrast sensitivity of the human eye," *Proc. SPIE* **5294**, 231–238 (2003).
26. M. J. Nadenau, J. Reichel, and M. Kunt, "Wavelet-based color image compression: exploiting the contrast sensitivity function," *IEEE Trans. Image Process.* **12**, 58–70 (2003).
27. J. Yao and G. Liu, "A novel color image compression algorithm using the human visual contrast sensitivity characteristics," *Photon. Sens.* **7**, 72–81 (2017).
28. W. S. Geisler and J. S. Perry, "Real-time foveated multiresolution system for low-bandwidth video communication," *Proc. SPIE* **3299**, 294–305 (1998).
29. A. Bozorgian, "MATLAB codes for models and evaluation," GitHub (2022), <https://github.com/alibzr/ModifiedBarten>.
30. P. G. Barten, *Contrast Sensitivity of the Human Eye and Its Effects on Image Quality* (1999).
31. J. Rovamo, O. Luntinen, and R. Näsänen, "Modelling the dependence of contrast sensitivity on grating area and spatial frequency," *Vision Res.* **33**, 2773–2788 (1993).
32. J. M. Rovamo, M. I. Kankaanpää, and H. Kukkonen, "Modelling spatial contrast sensitivity functions for chromatic and luminance-modulated gratings," *Vision Res.* **39**, 2387–2398 (1999).
33. S. J. Daly, "Visible differences predictor: an algorithm for the assessment of image fidelity," *Proc. SPIE* **1666**, 2–15 (1992).
34. J. A. Movshon and L. Kiorpes, "Analysis of the development of spatial contrast sensitivity in monkey and human infants," *J. Opt. Soc. Am. A* **5**, 2166–2172 (1988).
35. C. W. Thomas, G. C. Gilmore, and F. L. Royer, "Models of contrast sensitivity in human vision," *IEEE Trans. Syst. Man Cybern.* **23**, 857–864 (1993).
36. R. K. Mantiuk, M. Ashraf, and A. Chapiro, "stelaCSF—a unified model of contrast sensitivity as the function of spatio-temporal frequency, eccentricity, luminance and area," *ACM Trans. Graph.* **41**, 145 (2022).
37. G. M. Johnson and M. D. Fairchild, "On contrast sensitivity in an image difference model," in *IS and TS PICS Conference* (Society for Imaging Science & Technology, 2002), pp. 18–23.
38. S. Daly, "As plain as the noise on your face: adaptive video compression using face detection and visual eccentricity models," *J. Electron. Imaging* **10**, 30 (2001).
39. P. G. J. Barten, "The SQRI method: a new method for the evaluation of visible resolution on a display," *Proc. SID* **28**, 253–262 (1987).
40. H. Wassle and H. J. Riemann, "The mosaic of nerve cells in the mammalian retina," *Proc. R. Soc. London B* **200**, 441–461 (1978).
41. B. A. Szmajda, U. Grünert, and P. R. Martin, "Mosaic properties of midget and parasol ganglion cells in the marmoset retina," *Vis. Neurosci.* **22**, 395–404 (2005).
42. B. B. Lee, "Receptive field structure in the primate retina," *Vision Res.* **36**, 631–644 (1996).
43. N. Drasdo, C. L. Millican, C. R. Katholi, and C. A. Curcio, "The length of Henle fibers in the human retina and a model of ganglion receptive field density in the visual field," *Vision Res.* **47**, 2901–2911 (2007).
44. A. Papoulis, *Systems and Transforms with Applications in Optics*, McGraw-Hill Series in Systems Science (1968).
45. R. N. Bracewell, *The Fourier Transform and Its Applications* (McGraw-Hill, 1986), Vol. **31999**.
46. A. Roka, P. Galambos, and P. Baranyi, "Contrast sensitivity model of the human eye," in *ISCI 2009: 4th International Symposium on Computational Intelligence and Intelligent Informatics, Proceedings* (2009), Vol. **1**, pp. 93–99.
47. P. Lennie, J. Pokorny, and V. C. Smith, "Luminance," *J. Opt. Soc. Am. A* **10**, 1283 (1993).
48. R. Shapley and V. H. Perry, "Cat and monkey retinal ganglion cells and their visual functional roles," *Trends Neurosci.* **9**, 229–235 (1986).
49. W. H. Merigan and J. H. R. Maunsell, "How parallel are the primate visual pathways?" *Annu. Rev. Neurosci.* **16**, 369–402 (1993).
50. E. Kaplan, "The P, M and K streams of the primate visual system: what do they do for vision?" in *The Senses: A Comprehensive Reference* (2008), Chap. 1.16.
51. E. Kaplan, "The M, P and K pathways in the primate visual system," *New Vis. Neurosci.* **1**, 481–494 (2004).
52. A. Valberg, B. B. Lee, J. Pokorny, P. R. Martin, and V. C. Smith, "Luminance and chromatic modulation sensitivity of macaque ganglion cells and human observers," *J. Opt. Soc. Am. A* **7**, 2223–2236 (1990).
53. B. B. Lee, P. R. Martin, and A. Valberg, "The physiological basis of heterochromatic flicker photometry demonstrated in the ganglion cells of the macaque retina," *J. Physiol.* **404**, 323–347 (1988).
54. R. Shapley, "Visual sensitivity and parallel retinocortical channels," *Annu. Rev. Psychol.* **41**, 635–658 (1990).
55. L. N. Thibos, D. J. Walsh, and F. E. Cheney, "Vision beyond the resolution limit: aliasing in the periphery," *Vision Res.* **27**, 2193–2197 (1987).
56. M. O. Wilkinson, R. S. Anderson, A. Bradley, and L. N. Thibos, "Neural bandwidth of veridical perception across the visual field," *J. Vis.* **16**(2):1 (2016).
57. L. N. Thibos, F. E. Cheney, and D. J. Walsh, "Retinal limits to the detection and resolution of gratings," *J. Opt. Soc. Am. A* **4**, 1524–1529 (1987).
58. W. H. Merigan and L. M. Katz, "Spatial resolution across the macaque retina," *Vision Res.* **30**, 985–991 (1990).
59. D. M. Dacey, "The mosaic of midget ganglion cells in the human retina," *J. Neurosci.* **13**, 5334–5355 (1993).
60. A. B. Watson, "A formula for human retinal ganglion cell receptive field density as a function of visual field location," *J. Vis.* **14**(7):15 (2014).
61. J. P. Thomas, "Effect of eccentricity on the relationship between detection and identification," *J. Opt. Soc. Am. A* **4**, 1599–1605 (1987).
62. S. Polyak, *The Vertebrate Visual System* (University of Chicago, 1957), Vol. **277**.
63. "WebPlotDigitizer—Copyright 2010-2021 Ankit Rohatgi," <https://apps.automeris.io/wpd/>.
64. J. B. Jonas, U. Schneider, and G. O. H. Naumann, "Count and density of human retinal photoreceptors," *Graefes Arch. Clin. Exp. Ophthalmol.* **230**, 505–510 (1992).
65. E. V. Famiglietti and H. Kolb, "Structural basis for ON- and OFF-center responses in retinal ganglion cells," *Science* **194**, 193–195 (1976).
66. E. S. Yamada, L. C. L. Silveira, and V. H. Perry, "Morphology, dendritic field size, somal size, density, and coverage of M and P retinal ganglion cells of dichromatic Cebus monkeys," *Vis. Neurosci.* **13**, 1011–1029 (1996).
67. V. Virsu, P. Lehtio, and J. Rovamo, "Contrast sensitivity in normal and pathological vision," *Doc. Ophthalmol. Proc. Ser.* **30**, 263–272 (1981).
68. D. Lane, *Online Statistics Education: A Multimedia Course of Study* (Association for the Advancement of Computing in Education (AACE), 2003).
69. D. R. Williams, "Aliasing in human foveal vision," *Vision Res.* **25**, 195–205 (1985).
70. F. W. Campbell and R. W. Gubisch, "Optical quality of the human eye," *J. Physiol.* **186**, 558–578 (1966).
71. A. B. Watson, "Estimation of local spatial scale," *J. Opt. Soc. Am. A* **4**, 1579–1582 (1987).